Explanation of pressure-induced transformations in chain silicates based on their modular structures

2000 J. Phys.: Condens. Matter 12 8939

(http://iopscience.iop.org/0953-8984/12/42/301)

J. Phys.: Condens. Matter **12** (2000) 8939–8952. Printed in the UK PII: S0953-8984(00)14329-2

Explanation of pressure-induced transformations in chain silicates based on their modular structures

G Serghiou†, A Chopelas†‡ and R Boehler†

† Max-Planck Institute for Chemistry, Postfach 3060, Mainz 55020, Germany
‡ Department of Physics, University of Nevada, Box 454002, Las Vegas, NV 89154, USA

Received 30 May 2000, in final form 1 August 2000

Abstract. Above 35 GPa tetrahedrally coordinated (SiO_4) chain silicates either become amorphous or transform to dense crystalline phases that generally contain SiO_6 octahedra, depending on the sequencing of their building blocks (P and C modules). Previous work shows that the P and C modules are respectively slabs of the pyroxene and $CaSiO_3$ chain silicate structures. Chain silicates containing only P modules (e.g. the pyroxenes $MgSiO_3$, $Ca_{0.5}Mg_{0.5}SiO_3$, $MnSiO_3$) transform to dense crystalline phases. Chain silicates containing a sequence of P and C modules (e.g. the pyroxenoid $MnSiO_3$) become amorphous, and those containing only C modules (e.g. the pyroxenoid $CaSiO_3$) exhibit both crystalline and amorphous regions. Amorphization is likely to be triggered by disordering of the C modules and C–P interfaces, both of which become unstable with respect to P modules and P–P interfaces upon compression. The absence of C–P interfaces may explain the existence of both crystalline and amorphous regions in chain silicates containing only C modules.

1. Introduction

Crystalline to non-crystalline transitions upon compression can be studied at ambient temperature, thus allowing for a detailed examination of the mechanism of such transitions [1–3]. A majority of studies in this area focus on the tetrahedrally coordinated polymorphs of SiO_2 [1, 4, 5]. Under hydrostatic conditions, at ambient temperature, quartz transforms to a new crystalline phase at 21 GPa which becomes amorphous above 30 GPa [6, 7]. Recent molecular dynamics simulations find that the new phase consists of distorted SiO_x polyhedra, with x ranging from four to six [8]. Likewise, coesite, the denser tetrahedrally coordinated polymorph of SiO_2, stable above 3 GPa, becomes amorphous above 30 GPa [6]. Molecular dynamic calculations indicate that with increasing pressure the Si–O coordination of the amorphized phases of quartz and coesite approaches six [1, 9]. The thermodynamically stable phase of silica above 10 GPa is stishovite [10] which is a dense octahedrally coordinated SiO_2 polymorph [11]. The transition of the lower density SiO_2 phases to stishovite though is kinetically impeded at ambient temperature. Amorphization in SiO_2 thus provides an alternative densification pathway via an increase in Si–O coordination that is accessible at ambient temperature [2].

While the SiO_2 system is an important prototype system for studying the crystal chemistry of silicates it does not contain structural attributes characteristic of the majority of silicate structures, namely, network modifier polyhedral units (MgO_x, CaO_x polyhedra) [12]. Introducing network modifiers, such as alkali or alkaline earth oxides, into the structure disrupts the fully polymerized Si–O tetrahedral network. This is because the oxygens are shared with

0953-8984/00/428939+14$30.00

adjacent polyhedra containing network-modifying ions (countercations), which are typically octahedrally coordinated to oxygen. The bonding type also becomes more varied since the network modifier bonds with oxygen are less directional (more ionic) than the Si–O bonds within the tetrahedra [13].

We focus, here, on the high pressure behaviour of three crystals of a large class of chain silicates which contain network modifiers, with the chemical formula ($AA'BO_3$; A, A′: Mg, Ca, Mn, Fe; B: Si). Like SiO_2 these solids appear both as crystals and as melt-quenched glasses allowing a direct comparison of pressure-induced disordered states with their melt-quenched glassy analogues. These tetrahedrally coordinated (SiO_4) chain crystals are also dominant structures at shallow depths in the Earth [14]. At greater depths (>670 km) where temperatures exceed 1800 K, the high pressure octahedrally coordinated (SiO_6) perovskite structure of $MgSiO_3$ is dominant [15].

Chain silicates consist of chains of corner connected SiO_4 tetrahedra which run parallel to the crystallographic *c*-axis. These chains are separated from each other by layers of edge shared A and A′ octahedra. Crystals within this family differ from each other largely by the periodicity of the tetrahedra within the chains (tetrahedral repeat) [16]. Crystals with a periodicity of 2 (e.g. $MgSiO_3$, $Ca_{0.5}Mg_{0.5}SiO_3$) are called pyroxenes whereas those with a periodicity larger than 2 (e.g. $CaSiO_3$—3, $MnSiO_3$—7) are called pyroxenoids. Previous work shows that these chain silicates consist of pyroxene (P) and pyroxenoid $CaSiO_3$ (C) modules [17] (figures 1(a), (b)). These modules are slabs of pyroxene and $CaSiO_3$ pyroxenoid structure. The pyroxene (P) and $CaSiO_3$ (C) modules have average thicknesses of two and three corner connected tetrahedral units respectively. The modules are stacked next to each other in the appropriate sequence along the direction of the tetrahedral chains. Pyroxenes and $CaSiO_3$ pyroxenoid consist of an infinite sequence of their respective modules (PPP . . . for pyroxenes and CCC . . . for $CaSiO_3$ pyroxenoid) (figures 1(c), (d)). $MnSiO_3$ pyroxenoid consists of an infinite sequence of CPP modules (CPPCPPCPP . . .) (figure 1(e)). The repeat unit in chain silicates reflects the periodicity of the tetrahedra in the chain (e.g. P is 2 for pyroxenes, C is 3 for $CaSiO_3$ pyroxenoid and CPP is $3+2+2 = 7$ for $MnSiO_3$ pyroxenoid). Transitions between pyroxenoids and pyroxenes are reconstructive, and high temperatures are required to convert pyroxenoids to pyroxenes upon compression [18, 19].

In this study pyroxenoids are compared to pyroxenes with respect to transitions from crystalline to non-crystalline states upon compression. Previous work on $MgSiO_3$ pyroxene indicates that pyroxenes do not become amorphous upon compression to the highest pressures studied of 70 GPa [20]. We first compare the compressional behaviour of the pyroxenoid $MnSiO_3$ with that of $MnSiO_3$ pyroxene converted from the pyroxenoid at 10 GPa and 1500 K and with that of a further pyroxene, $Ca_{0.5}Mg_{0.5}SiO_3$. We then extend our investigation to $CaSiO_3$ pyroxenoid.

We use Raman spectroscopy for monitoring the structural changes in our samples because this technique is sensitive to the structure of both crystalline and non-crystalline solids [13].

2. Experimental techniques

Single crystals of $MnSiO_3$ (triclinic, space group $P\bar{1}$, $Z = 14$; Minas Gerais, Brazil, mineral name: pyroxmangite), $CaSiO_3$ (triclinic, space group $P\bar{1}$, $Z = 6$; Karibib, Namibia, mineral name: wollastonite) and $Ca_{0.5}Mg_{0.5}SiO_3$ (monoclinic, space group $C2/c$, $Z = 4$; De Kalb, New York, mineral name: diopside) [21] were used for all experiments. Pressure was applied with a diamond anvil cell. The crystals, of dimensions 10 μm × 50 μm × 20 μm, were placed in the centre of 301 stainless steel gaskets in an argon pressure medium. The sample chamber dimensions were between 130 and 150 μm in diameter and 60 μm in thickness. The Raman

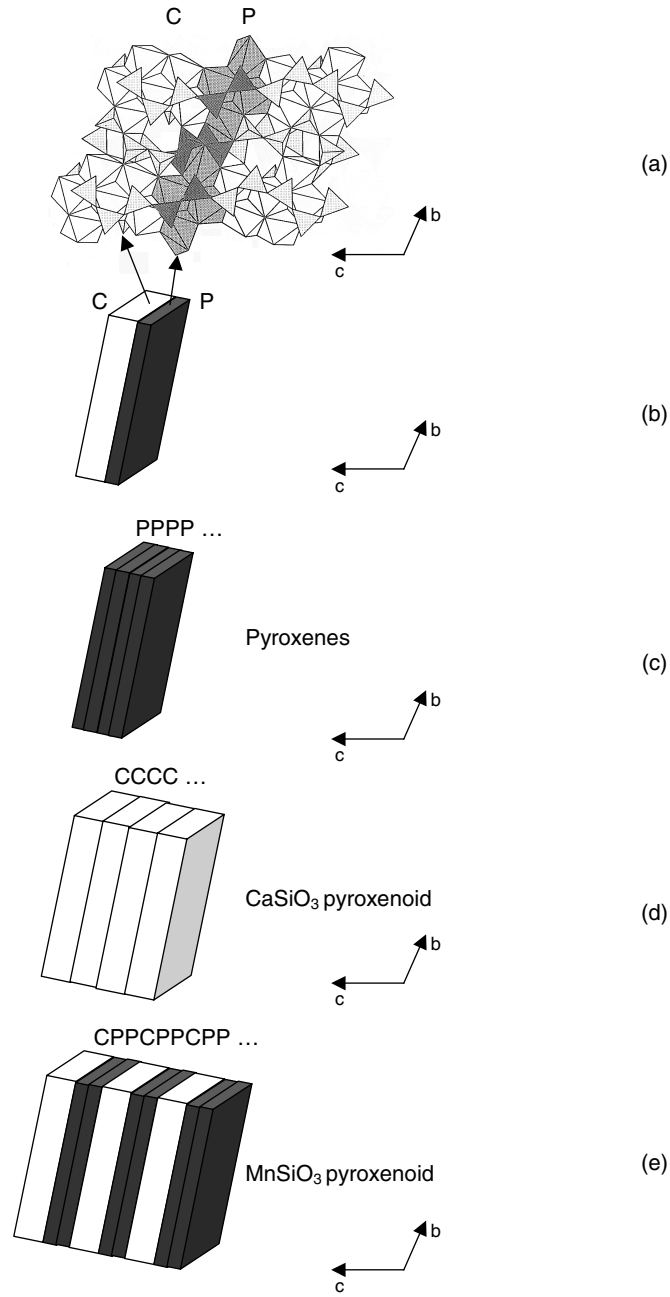

Figure 1. Polyhedral diagram of $MnSiO_3$ pyroxenoid projected onto the *b*–*c* plane (figure 1(a)) (figure 1(a) is reproduced by permission from [17]). The larger polyhedra indicate Mn–O octahedra and the smaller polyhedra (triangles) indicate SiO_4 tetrahedra. The chains of corner connected (SiO_4) tetrahedra (triangles) run along the crystallographic *c*-axis. A P module is indicated by the darker shading. A C module is also labelled in the figure. The P and C modules are also indicated schematically in terms of a shaded and a transparent slab respectively (figure 1(b)). The slabs are stacked next to each other along the *c*-axis. The structure of pyroxenes consists of an infinite sequence of P modules (figure 1(c)), that of $CaSiO_3$ pyroxenoid of an infinite sequence of C modules (figure 1(d)) and that of $MnSiO_3$ pyroxenoid of an infinite sequence of CPP modules (figure 1(e)).

spectra were excited with the 457.9 nm line of an argon ion laser with powers ranging from 5 to 30 mW. The Raman spectra were analysed with a Spex 1402 double monochromator with a LN-cooled CCD (charged coupled device detector). The defocused beam of a 120 watt continuous wave CO_2 laser [22] was used for heating the $MnSiO_3$ samples at high pressure in order to convert the $MnSiO_3$ pyroxenoid into its pyroxene analogue. Heating durations were about 20 minutes at temperatures of about 1500 K. Pressure was measured using micron sized ruby chips placed next to the samples. $CaSiO_3$ glass was synthesized from a finely ground and intimately mixed stoichiometric CaO and SiO_2 mixture which was placed on a platinum plated copper disc and subsequently melted using a CO_2 laser, followed by splat-quenching with a second platinum plated copper disc.

3. Results

3.1. Raman measurements

The high pressure Raman spectra of crystalline $MnSiO_3$, $Ca_{0.5}Mg_{0.5}SiO_3$ and $CaSiO_3$ are shown in figures 2, 3 and 4 respectively. The ambient pressure spectra of the three chain structures span the region from 200 to 1200 cm^{-1}. The vibrational modes can be classified into three regimes. The regime below 600 cm^{-1} consists of modes associated with countercation (Mn–O, Ca–O, Mg–O) stretches, internal O–Si–O bending, as well as longer wavelength lattice modes. The peaks in the midfrequency region between 600 and 800 cm^{-1} are due to Si–O–Si intertetrahedral stretching and bridging modes, whereas the bands at higher wavenumbers are due to Si–O stretching modes of the non-bridging oxygens in the silica tetrahedra [23, 24].

3.2. $MnSiO_3$ pyroxenoid

The structure of $MnSiO_3$ undergoes three modifications at 4, 17 and 28 GPa. But the most important transition in the context of our study occurs above 35 GPa where all Raman modes vanish, indicating formation of a disordered or amorphous state (figure 2(a)). Measurements were taken during decompression but the spectrum remains featureless until the sample is recovered outside the diamond cell. The release spectrum was taken using a 5 mW defocused beam to ensure that the sample would not be heated. This spectrum, shown at the top of figure 2(a), is characteristic of amorphous solids, and is similar to that of melt-quenched glasses in this family [25]. The results shown in figure 2(a) were reproduced in three different experiments under the same conditions.

In the next set of experiments we use $MnSiO_3$ pyroxenoid that was converted to a clinopyroxene at 10 GPa and about 1500 K, consistent with previous work [18]. Above 40 GPa, the clinopyroxene converts to a new crystalline phase which remains stable to the highest pressures examined (63 GPa). The spectrum of the new phase differs substantially from that of the lower pressure tetrahedrally coordinated $MnSiO_3$ polymorphs (figure 1(b)). Most importantly, its highest energy mode lies between that observed for tetrahedrally (SiO_4) and octahedrally (SiO_6) coordinated polymorphs in the ($AA'BO_3$; A, A′: Mg, Ca, Mn, Fe; B: Si) family (see section 3.5). Upon decompression the clinopyroxene phase reappears at 19 GPa and is recoverable to ambient pressure and temperature conditions (figure 2(b)).

3.3. $Ca_{0.5}Mg_{0.5}SiO_3$ pyroxene

The $Ca_{0.5}Mg_{0.5}SiO_3$ structure undergoes a subtle isosymmetric phase transition from the ambient temperature and pressure $C2/c$ phase to the high pressure $C2/c$ phase at about 5 GPa and room temperature [26]. In two experiments the structure undergoes a polymorphic

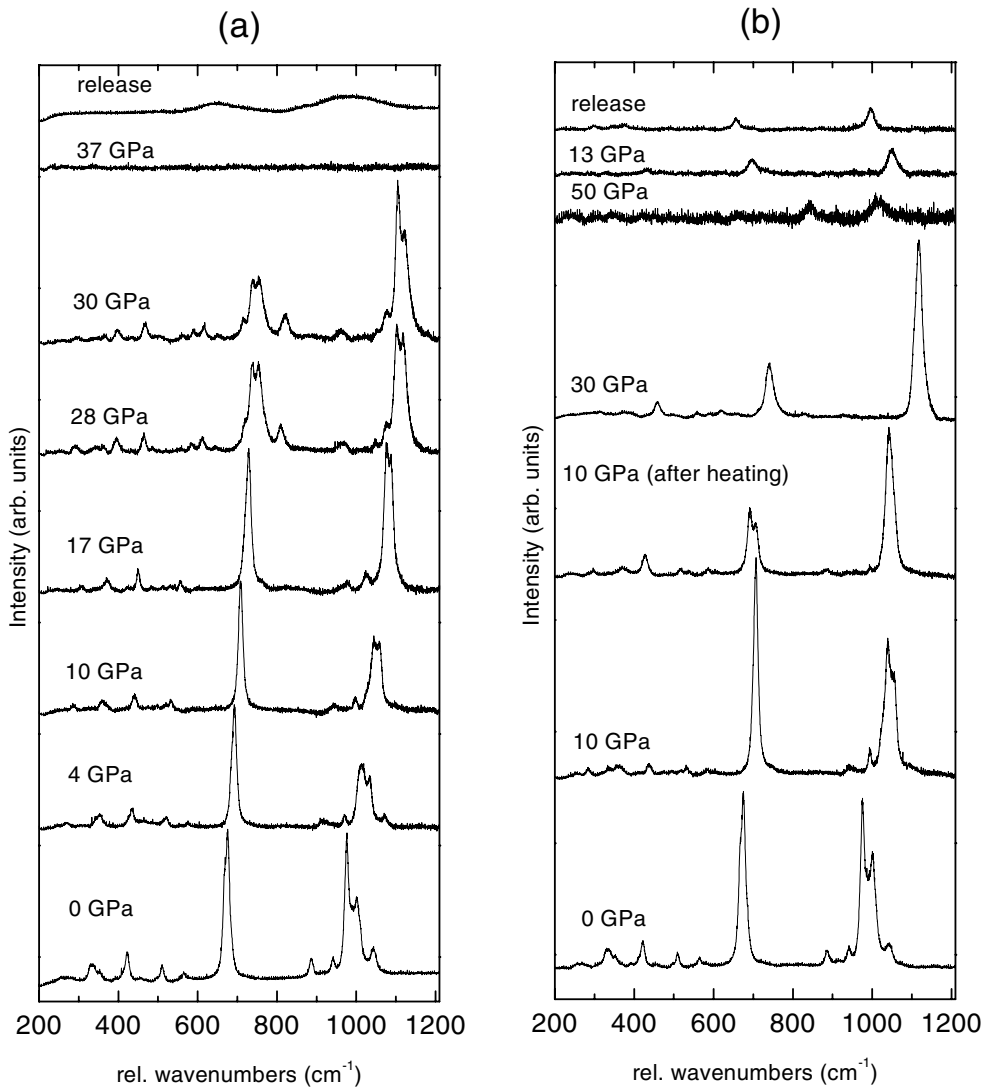

Figure 2. Effect of pressure on the Raman spectrum of crystalline $MnSiO_3$ showing evidence for a crystal–amorphous transition above 35 GPa (figure 2(a)). The spectrum of the recovered phase resembles that of melt-quenched chain silicate glasses. $MnSiO_3$ clinopyroxene, synthesized from $MnSiO_3$ pyroxenoid at 10 GPa and 1500 K does not become amorphous at higher pressures (figure 2(b)). Above 40 GPa, the clinopyroxene phase transforms instead to a new crystalline phase which remains stable to the highest pressures measured of 63 GPa. Upon release of pressure this new crystalline phase reverts back to the clinopyroxene phase at about 20 GPa, which at ambient pressure has a Raman spectrum similar to that of the $C2/c$ phase of $Ca_{0.5}Mg_{0.5}SiO_3$ (figure 2(b)).

transition to a new phase at about 55 GPa, which also contains SiO_4 units as seen by the stretching mode indicated by an arrow in figure 3. At 59 GPa, this tetrahedrally coordinated phase transforms to a new crystalline structure containing only SiO_6 units indicated by an arrow in figure 3 (see section 3.5). However in two further experiments on crystals subjected to the same conditions as in our first two experiments, tetrahedrally coordinated (SiO_4) units

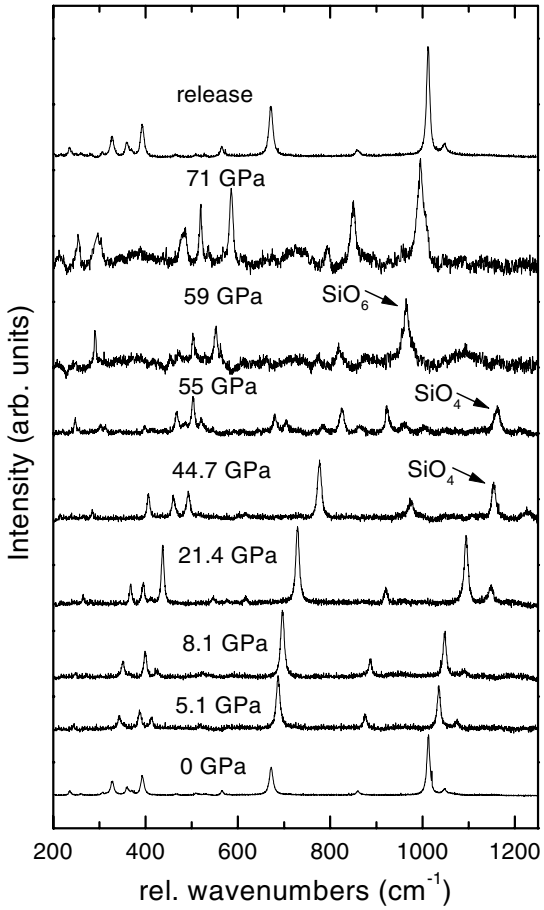

Figure 3. Effect of pressure on the Raman spectrum of crystalline $Ca_{0.5}Mg_{0.5}SiO_3$ showing evidence for a transition to a new phase at room temperature and about 55 GPa which also contains tetrahedral units. Above 55 GPa the stretching vibrations associated with the tetrahedrally coordinated phase vanish and new modes associated with an (SiO_6) octahedrally coordinated phase appear.

of $Ca_{0.5}Mg_{0.5}SiO_3$ persist to pressures higher than 59 GPa. Previous CO_2 laser-heating experiments on $MgSiO_3$ pyroxene indicate that the SiO_4 to SiO_6 coordination change in the crystal is facilitated by defects in the structure [20]. Above 7 GPa at room temperature, $MgSiO_3$ pyroxene exists as a mixed phase consisting of ortho and clinopyroxene [23]. Pure clinopyroxene was synthesized by heating the mixed ortho/clinopyroxene phase to 2000 K using a CO_2 laser at 16 GPa. While a new phase appears above 40 GPa at room temperature, SiO_4 tetrahedral units persist to the highest pressures measured (47 GPa). This is in contrast to unheated $MgSiO_3$ pyroxene where the tetrahedral stretching modes (SiO_4) vanish, and are replaced by octahedrally coordinated (SiO_6) modes between 38 and 47 GPa at room temperature. This observation indicates that defects such as grain boundaries at the interface of the ortho and clinopyroxene structures, may provide nucleation centres that make the tetrahedral to octahedral transition in $MgSiO_3$ more accessible. 'Annealing' the structure to the pure clinopyroxene phase minimizes or eliminates defects (nucleation centres) in the

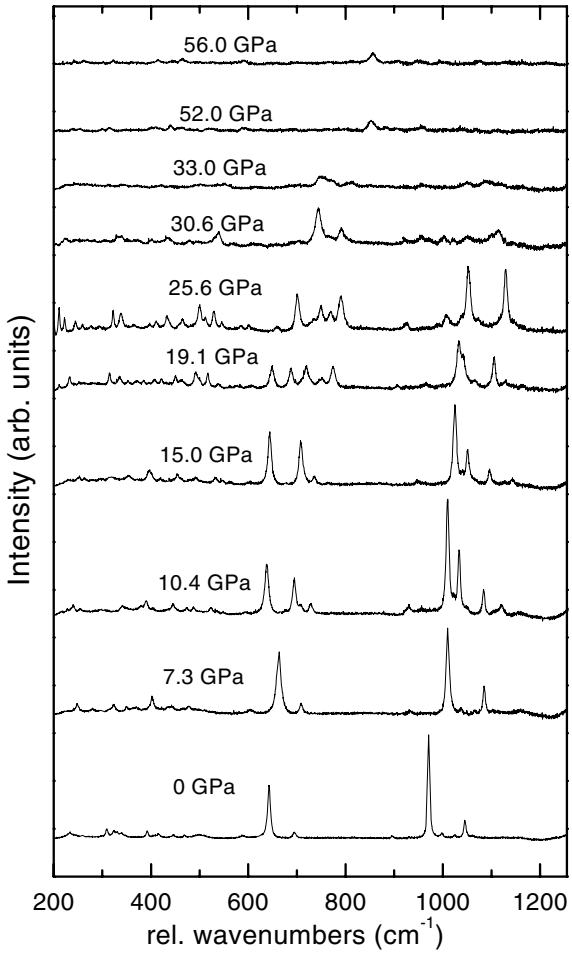

Figure 4. Effect of pressure on the Raman spectrum of crystalline $CaSiO_3$ showing evidence for four phase transitions at 7, 10, 19 and 30 GPa. Above 40 GPa all modes vanish except in a small region of the sample where, reproducibly, new modes around 800 cm^{-1} appear indicative of a coordination change to a phase containing SiO_6 units.

structure which arguably explains the persistence of tetrahedrally coordinated Si–O units upon further compression to 47 GPa. Likewise, in $Ca_{0.5}Mg_{0.5}SiO_3$ pyroxene the observed ease or sluggishness of the tetrahedral (SiO_4) to octahedral (SiO_6) coordination change above 59 GPa may be dependent on the presence and creation of defects in the $Ca_{0.5}Mg_{0.5}SiO_3$ structure upon ambient temperature compression. Important is that in all experiments the new structures remain crystalline to the highest pressures of our measurements (71 GPa) and revert back to the ambient pressure crystal phase upon release (figure 3).

In synopsis both the $MgSiO_3$ and $Ca_{0.5}Mg_{0.5}SiO_3$ pyroxenes as well as the pyroxene phase of $MnSiO_3$ in contrast to their unheated $MnSiO_3$ pyroxenoid analogue remain crystalline upon compression to the highest pressures of our studies.

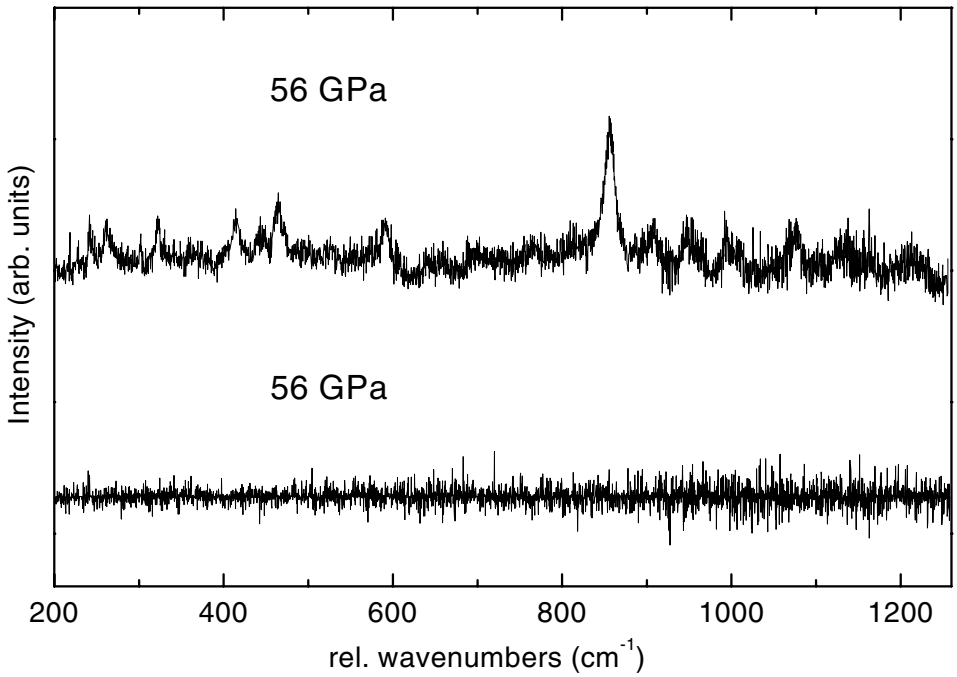

Figure 5. Raman spectra of $CaSiO_3$ at 56 GPa from the portion of the sample where the new modes appeared (top) and from the remainder of the sample whose Raman spectrum became featureless (bottom).

3.4. $CaSiO_3$ pyroxenoid

The $CaSiO_3$ structure undergoes four phase transitions between tetrahedrally coordinated (SiO_4) structures at 7, 10, 19 and 30 GPa. The presence of the SiO_4 units is evident from the vibrational bands associated with Si–O tetrahedral stretching modes above 950 cm wavenumbers (figure 4). Above 40 GPa a new Raman mode belonging to an octahedrally coordinated (SiO_6) phase appears (figure 4, figure 5 top spectrum) (see also section 3.5). The new crystalline phase only occurs in a region of about 20 μm diameter in the sample. In the remainder of the sample, the spectrum is featureless, indicative of a disordered or amorphous phase (figure 5, bottom spectrum). These observations were made reproducibly in three experiments. In a fourth experiment however, above 40 GPa, the spectrum became featureless throughout the sample. The release spectrum from the regions of the sample whose spectrum is featureless above 40 GPa, strongly resembles that of melt-quenched $CaSiO_3$ glass (figures 6(a), (b)). The Raman spectrum at ambient pressure, after melting $CaSiO_3$ perovskite at 40 GPa, is also very similar to that of the other amorphous phases (figure 6(c)) [27]. Moreover, the major Raman modes of the ambient pressure chain structure are recovered after pressure release from the region where the octahedrally coordinated $CaSiO_3$ phase appears above 40 GPa (figure 7).

3.5. Coordination changes

Coordination changes in chain structures at room temperature were described previously for $MgSiO_3$ [20]. Here we extend that work with our present results on $Ca_{0.5}Mg_{0.5}SiO_3$, $CaSiO_3$ and $MnSiO_3$. At 59 GPa the frequency bands of the tetrahedrally (SiO_4) coordinated structure of $Ca_{0.5}Mg_{0.5}SiO_3$ vanish, and vibrational bands belonging to an octahedrally (SiO_6)

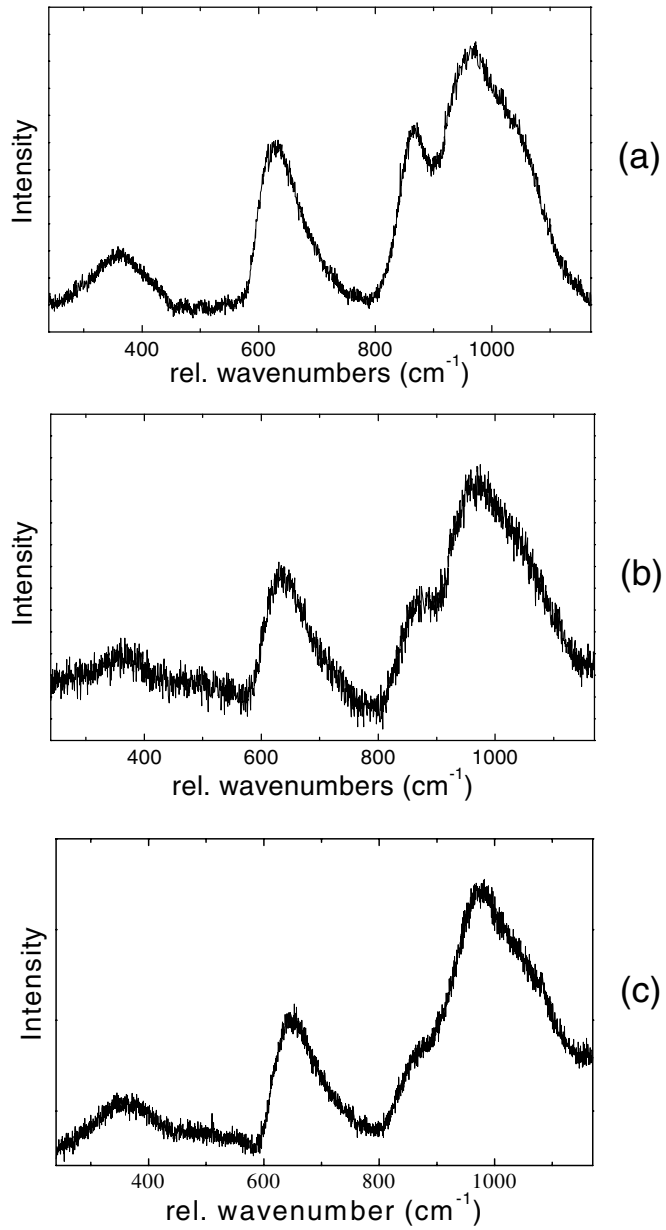

Figure 6. Raman spectrum of (a) melt-quenched $CaSiO_3$ glass at 1 atm, of (b) the recovered sample from those portions of the sample whose spectrum became featureless at high pressure and (c) from a recovered $CaSiO_3$ sample after it was melted at about 4200 K and 40 GPa. It is noteworthy that the local to medium range order structure (5–20 Å) of the recovered amorphous samples are very similar even though they were prepared in different ways. The disordering of $CaSiO_3$ upon compression and its similarity to melt-quenched $CaSiO_3$ glass may also be related to the polytypic behaviour of the $CaSiO_3$ crystal [39] described previously [37].

coordinated phase appear. The SiO_6 non-bridging stretching modes (indicated by an arrow in figure 3) appear two hundred wavenumbers lower than the SiO_4 non-bridging stretching modes

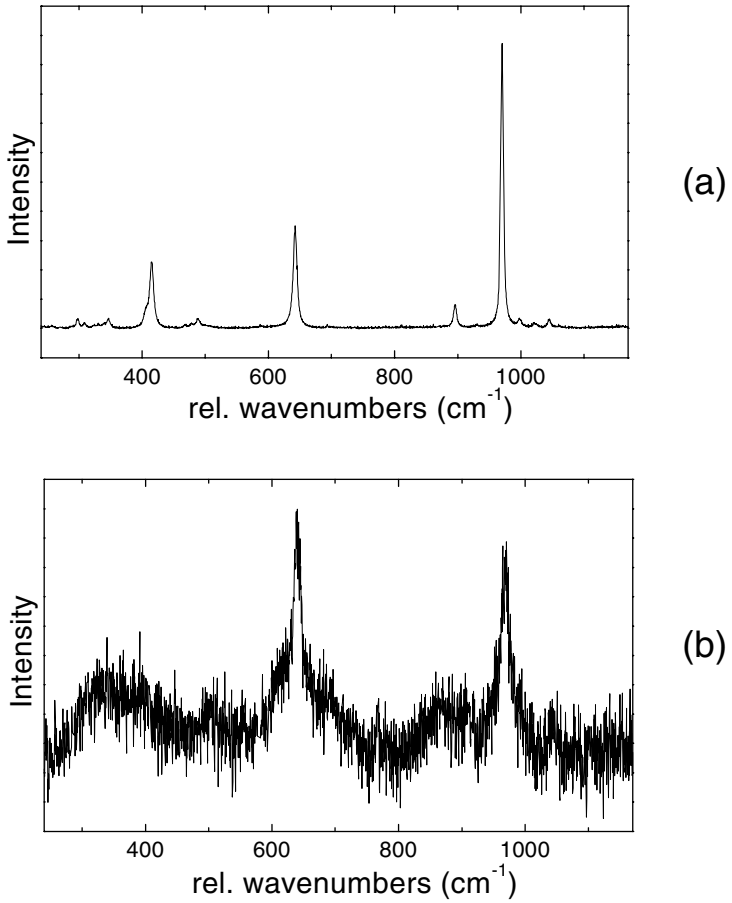

Figure 7. Raman spectra of a $CaSiO_3$ crystal at ambient pressure (figure 7(a)) and of the recovered $CaSiO_3$ sample (figure 7(b)) from 56 GPa from that portion of the sample that remained crystalline at all pressures. The strongest Raman modes of the ambient pressure $CaSiO_3$ phase were recovered upon release of pressure.

(indicated by an arrow in figure 3) (figure 8). We assign the most intense, high wavenumber mode at 71 GPa to a stretching vibration of SiO_6 octahedral units, because its position and pressure dependency is very similar to that of the intense Si–O stretching vibration of SiO_6 units in $MgSiO_3$ ilmenite [20, 22]. In addition, octahedral stretching vibrations (SiO_6) in the same frequency regime are observed in the infrared spectra of $MgSiO_3$ perovskite [28]. The mechanism for the SiO_4–SiO_6 coordination change in $Ca_{0.5}Mg_{0.5}SiO_3$ likely involves a tilting of the tetrahedral units towards each other within the chains in accordance with the polyhedral tilt model developed to explain four to six coordination changes in silicate glasses [29]. This mechanism is also reported to occur in the first order phase transition of α-quartz to a higher coordinated crystalline phase under hydrostatic compression at 21 GPa [8]. Based on this polyhedral tilt model, the new high pressure phase synthesized here consists of chains of edge sharing SiO_6 octahedra which differs both from ilmenite, which contains layers of edge connected Si–O octahedra and perovskite, which contains a three-dimensional network of corner connected Si–O octahedra [11]. The reconstructive changes required for a transition to

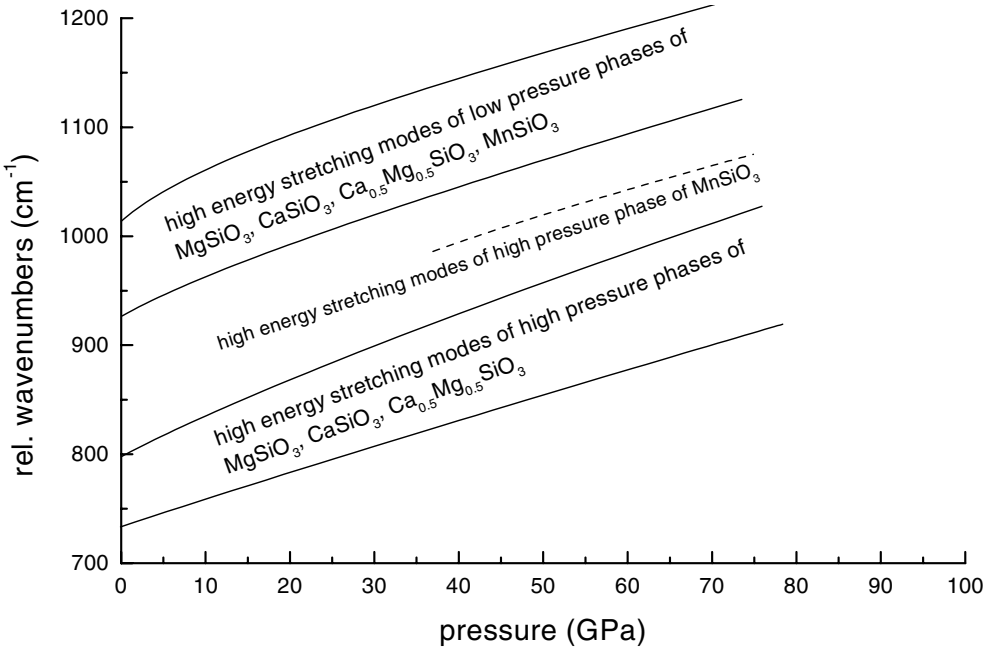

Figure 8. Wavenumber regime where the highest energy Si–O tetrahedral stretches of $MnSiO_3$, $CaSiO_3$, $Ca_{0.5}Mg_{0.5}SiO_3$, $MgSiO_3$ appear. Also shown is the wavenumber regime where the highest energy Si–O stretches of $MgSiO_3$, $Ca_{0.5}Mg_{0.5}SiO_3$, $CaSiO_3$ appear after the crystals transform to their higher density polymorphs at high pressure and ambient temperature. We assign this latter regime to Si–O octahedral stretching vibrations because the position and pressure dependency of the intense Si–O stretching vibrations of SiO_6 units in $MgSiO_3$ ilmenite [20] and the infrared active octahedral stretching vibrations of $MgSiO_3$ perovskite [28] also occur in this frequency regime. In contrast as shown in the figure, the highest frequency Si–O stretching vibrations of the new dense phase of $MnSiO_3$ (figure 1(b)) fall in an area between the SiO_4 and SiO_6 coordination regimes and thus any further assigment must await *in situ* x-ray diffraction work. $MnSiO_3$ does not have an ilmenite phase in its pressure–temperature stability field so its spectrum cannot be compared to that presently obtained. We note that the position and pressure dependency of the Raman bands of $MnSiO_3$ garnet are different than those of the new phase observed here for $MnSiO_3$.

the 2D ilmenite type structure and even more so to the 3D perovskite structure are not likely at ambient temperature and high pressure.

Based on the positions of the non-bridging Si–O stretching vibrations of $CaSiO_3$, below and above 40 GPa (figure 8), this crystal also undergoes an SiO_4–SiO_6 coordination change above 40 GPa. The coordination change only occurs in a small region of the sample whereas the remainder becomes amorphous (see section 4). By comparison $MnSiO_3$ in the pyroxenoid form undergoes a crystal–amorphous transition at about 35 GPa throughout the sample. In contrast, the pyroxene phase of $MnSiO_3$ transforms above 40 GPa to a new crystalline phase. The SiO_4 non-bridging stretching vibrations of the pyroxene are replaced above 40 GPa by an Si–O stretching mode located at 1020 cm^{-1} at 50 GPa. The position of this mode at 50 GPa, and at all other pressures examined is between those expected for SiO_4 and SiO_6 coordination (figure 8). $MnSiO_3$ does not have an ilmenite phase at high pressures, but rather a garnet phase (a structure containing Mn–O dodecahedra, Mn–O and Si–O octahedra and Si–O tetrahedra) [30]. The garnet phase is stable at pressures above 13 GPa at about 1800 K. We synthesized $MnSiO_3$ garnet at 18 GPa and 1500 K. The garnet Raman spectrum is not the same

as that of the new $MnSiO_3$ phase stable above 40 GPa at room temperature. At 50 GPa the mid- and high frequency modes of $MnSiO_3$ garnet are at 748 and 1070 cm^{-1} whereas those of our new phase are at 842 and 1020 cm^{-1}. Upon the release of pressure the new $MnSiO_3$ phase reverts to the clinopyroxene structure whose Raman spectrum (figure 2(b) top spectrum) is similar to that of the $C2/c$ phase of $Ca_{0.5}Mg_{0.5}SiO_3$ pyroxene (figure 3 bottom spectrum) [22]. A further examination of the new crystalline phase of $MnSiO_3$ will require high resolution *in situ* x-ray diffraction measurements due to the non-quenchable nature of this phase.

4. Discussion

The results of this study, and our previous work on $MgSiO_3$ [20], show that the high pressure behaviour of pyroxenes differs from that of their pyroxenoid analogues. The structural interrelationships between pyroxenoids and pyroxenes [17] (see section 1) and the effect of compositional variation on their crystal structures [31], provides insight into why they respond differently to pressure.

Decreasing the countercation size in pyroxenoids (with pressure or composition) favours formation of the pyroxene structure [16]. This is most evident from a study of the crystal structures of several $Mn_xMg_{1-x})SiO_3$ pyroxenoid compositions [31]. This study reveals *where* in the pyroxenoid structure distortions occur as smaller magnesium countercations replace manganese countercations (as x decreases). The pyroxene (P) modules remain largely undistorted as x decreases. The pyroxenoid (C) modules on the other hand become increasingly distorted as x decreases. These distortions involve (a) kinks in the tetrahedral chains near the C–P boundary, (b) a decrease of non-bonded Si–Si distances below energetically favourable limits (<3.0 Å) [32] and (c) deformation of octahedral units in the C module [31]. Thus, both C–P interfaces and C modules become unstable with respect to P–P interfaces and P modules as the average countercation size in the slabs decreases. Therefore a pure pyroxene (PPP . . .) structure becomes favourable as countercation size decreases (or as external pressure increases). Previous work shows [19, 33] that the pyroxenoid–pyroxene transition is reconstructive, involving breaking and reforming of Si–O and (Mg, Mn, Ca)–O bonds and redistribution of cations. Incomplete pyroxenoid–pyroxene transformation results in the formation of disordered structures [34, 35]. These disordered structures are documented in a transmission electron microscopy (TEM) study on a natural sample containing both pyroxene and pyroxenoid structures [34]. Electron diffraction patterns and high resolution images from the sample reveal extensive chain periodicity faults and disordered intergrowths of pyroxenoids of different chain periodicities. Moreover, the transmission electron microscopy work shows that the pyroxene–pyroxenoid transition occurs both by growth of thin lamellae (a few Ångströms) and via a broad (up to several microns) reaction front. Thus, structural disordering due to incomplete conversion between pyroxene and pyroxenoid occurs in the natural sample on a few Ångströms to several micron length scales.

Both previous [18] and the present high pressure study show that the transformation of $MnSiO_3$ pyroxenoid to pyroxene requires high temperatures. Pressure generally decreases the size of the countercation polyhedra as compared to the size of the relatively incompressible SiO_4 tetrahedra [36]. Thus, ambient temperature compression of $MnSiO_3$ pyroxenoid results in distortions in the pyroxenoid structure similar to those described above when smaller magnesium ions replace manganese ions in the structure [31]. These distortions may cause transition to a chain structure of lower symmetry or to a disordered mixture of several chain structures as observed above for a natural sample using TEM measurements [34]. Lowering of symmetry (lifting of degeneracy of vibrational modes) or presence of a mixed phase would generally result in an increased number of Raman active modes. In $MnSiO_3$ this is consistent

with the replacement of a single Raman mode in the 600 to 800 wavenumber region at 17 GPa by at least four Raman modes at 28 GPa (figure 1(a)). Above 30 GPa at ambient temperature, transition to a new crystalline phase is kinetically impeded, resulting instead in an amorphous phase as shown by our Raman measurements on the unheated $MnSiO_3$ sample (figure 1(a)). We propose that the absence of pyroxenoid (C) modules and C–P linkages in the pure (PPP . . .) stacking sequence of the pyroxenes $MnSiO_3$, $MgSiO_3$ and $Ca_{0.5}Mg_{0.5}SiO_3$ allows these structures to accommodate higher pressures without becoming amorphous. Instead they transform to denser crystalline structures as described in the previous section.

$CaSiO_3$ like its $MnSiO_3$ pyroxenoid analogue becomes amorphous above 40 GPa. The amorphization in three of four experiments does not occur throughout the $CaSiO_3$ sample. A new octahedrally coordinated (SiO_6) crystalline phase is also present in a small region of the sample (figure 5). The reason for the presence of both amorphous and octahedrally coordinated crystalline regions above 40 GPa in $CaSiO_3$ may be traced back to its sequencing. As discussed above, both C modules and C–P interfaces contribute to the disordering of $MnSiO_3$ pyroxenoid upon compression. $CaSiO_3$ (CCC . . .) unlike $MnSiO_3$ (CPP . . .) pyroxenoid does not contain C–P linkages, which may allow formation of the denser crystalline phase above 40 GPa.

Phase transitions in $CaSiO_3$ pyroxenoid are also sensitive to pressure gradients. This is documented by a previous high pressure x-ray diffraction and Raman spectroscopic study of $CaSiO_3$ embedded in a pressure medium (4:1 methanol:ethanol) that becomes non-hydrostatic above 10 GPa. Under those conditions $CaSiO_3$ becomes amorphous at 26 GPa [37]. In argon at about 50 GPa the existing small pressure gradients (between 1 to 2 GPa) across the sample might enhance conversion to an amorphous state. That is, the new dense crystal may form in that part of the sample where the pressure gradients are smallest (the flattest part of the pressure distribution profile) whereas the remainder of the sample becomes amorphous. This can be tested in future experiments by measuring detailed pressure profiles (with 1–2 micron steps) across the sample at high pressure. In this way we can check whether the new crystalline phase emerges in the region of the sample where the pressure gradients are smallest. Amorphization in the pyroxenoid may also be enhanced by the transition to the dense crystalline phase. This is because crystal–crystal phase transitions in silicates involving SiO_4–SiO_6 coordination changes can result in density increases of the order of fifty per cent [38]. Amorphization of $CaSiO_3$ may then at least in part be caused by internal strain in the sample due to a large volume decrease in the region of the phase transition.

5. Conclusions

This work identifies trends for the pressure-induced phase transformations of an extended family of chain structures. Upon compression pyroxenes undergo transitions to octahedrally coordinated (SiO_6) crystalline phases whereas their longer period modulated pyroxenoid forms become amorphous. The amorphization process is triggered by kinetically impeded pyroxenoid (C module and C–P interface) to pyroxene (P module) transitions. The structures of the recovered pressure-amorphized samples are similar to those of their melt-quenched glassy analogues on the local to medium range order level (5–20 Å). Moreover we suggest that in pyroxenes [20] the presence of defects facilitates transition to octahedrally coordinated crystalline phases, while in pyroxenoids [37], internal strains caused by local volume decreases (phase transitions), as well as external stresses (pressure gradients), may promote crystal–amorphous transitions. Furthermore this work illustrates the importance of describing phase transitions in complex solids both on the local (polyhedral) and the medium to long range (modular) structural level. Finally previous observations that the onset of pressure-induced

amorphization occurs along distinct crystallographic directions [4], may be studied based on disordering at the interfaces of structural modules.

Acknowledgments

We thank Laurence Nigay, Matthew Kilburn and Daniel Errandonea for many helpful comments on the manuscript.

References

[1] Dean D W, Wentzcovitch R M, Keskar N, Chelikowsky J R and Bingelli N 2000 *Phys. Rev.* B **61** 3303–9
[2] Sharma S M and Sikka S K 1996 *Progr. Mater. Sci.* **40** 1–77
[3] Serghiou G, Reichmann H-J and Boehler R 1997 *Phys. Rev.* B **55** 14 765–9
[4] Kingma R J, Meade C, Hemley R J, Mao H K and Veblen D R 1993 *Science* **259** 666–9
[5] Somayazulu M S, Sharma S M and Sikka S K 1994 *Phys. Rev. Lett.* **73** 98–101
[6] Hemley R J, Jephcoat A P and Mao H K 1998 *Nature* **334** 52–4
[7] Kingma K J, Hemley R J, Mao H K and Veblen D R 1993 *Phys. Rev. Lett.* **70** 3927–30
[8] Wentzcovitch R M, da Silva C, Chelikowsky J R and Bingelli N 1998 *Phys. Rev. Lett.* **80** 2149–52
[9] Tse J S and Klug D D 1991 *Phys. Rev. Lett.* **67** 3559–62
[10] Serghiou G, Zerr A, Chudinovskikh L and Boehler R 1995 *Geophys. Res. Lett.* **22** 441–4
[11] Finger L W and Hazen R M 1991 *Acta. Crystallogr.* B **47** 561–80
[12] Gaskell P H, Eckersley M C, Barnes A C and Chieux P 1991 *Nature* **350** 675–7
[13] Wolf G H, Durben D J and McMillan P F 1990 *J. Chem. Phys.* **93** 2280–8
[14] Angel R J, Chopelas A and Ross N L 1992 *Nature* **358** 322–4
[15] Knittle E and Jeanloz R 1987 *Science* **257** 668–70
[16] Liebau F 1985 *Chemistry of Silicates* (Berlin: Springer)
[17] Angel R J and Burnham C W 1991 *Am. Mineral.* **76** 900–3
[18] Akimoto S and Syono Y 1972 *Am. Mineral.* **57** 76–84
[19] Angel R J, Price G D and Putnis A 1984 *Phys. Chem. Miner.* **10** 236–43
[20] Serghiou G, Boehler R and Chopelas A 2000 *J. Phys.: Condens. Matter* **12** 236–43
[21] Deer W A, Howie R A and Zussman J 1967 *Rock-Forming Minerals* (London: Longmans)
[22] Boehler R and Chopelas A 1992 *High-Pressure Research: Application to Earth and Planetary Sciences* ed Y Syono and M H Manghnani (Tokyo: Terra)
[23] Hugh-Jones D, Chopelas A and Angel R 1997 *Phys. Chem. Miner.* **24** 301–10
[24] Handke J 1986 *Appl. Spectrosc.* **40** 871–7
[25] Tsunawaki Y, Iwamoto N, Hattori T and Mitsuiki A 1981 *J. Non-Cryst. Solids.* **44** 369–78
[26] Ohlert J M and Chopelas A 1999 *EOS Trans.* **80** 928
[27] Zerr A, Serghiou G and Boehler R 1997 *Geophys. Res. Lett.* **24** 909–12
[28] Lu R, Hofmeister A M and Wang Y 1994 *J. Geophys. Res.* **99** 11 795–804
[29] Jeanloz R 1988 *Nature* **332** 207
[30] Fujino K, Momoi H, Sawamoto H and Kumuzawa M 1986 *Am. Mineral.* **71** 781–5
[31] Pinckney L R and Burnham C W 1988 *Am. Mineral.* **73** 798–808
[32] Hill R J and Gibbs G V 1979 *Acta Crystallogr.* B **35** 25–30
[33] Prewitt C T and Peacor D R 1964 *Am. Mineral.* **49** 1527–42
[34] Veblen D R 1985 *Am. Mineral.* **70** 885–901
[35] Veblen D R, Banfield J F, Guthrie G D, Heaney P J, Ilton E S, Livi K J T and Smelik E A 1993 *Science* **260** 1465–72
[36] Hazen R M and Finger L W 1982 *Comparative Crystal Chemistry* (New York: Wiley)
[37] Serghiou G and Hammack W S 1993 *J. Chem. Phys.* **98** 9830–4
[38] Smyth J R and McCormick T C 1995 *Mineral Physics and Crystallography. A Handbook of Physical Constants* ed T J Ahrens (Washington, DC: American Geophysical Union)
[39] Price G D and Yeomans Y 1984 *Acta Crystallogr.* B **40** 448–54